

# Joint Device Identification, Channel Estimation, and Signal Detection for LEO Satellite-Enabled Random Access

Bo Xiaohu Shen, Yongpeng Wu, Wenjun Zhang, Symeon Chatzinotas, and Börn Oersteren

**Abstract**—This paper investigates joint device identification, channel estimation, and signal detection for LEO satellite-enabled grant-free random access, where a multiple-input multiple-output (MIMO) system with orthogonal time-frequency space modulation (OTFS) is utilized. OTFS combats the dynamics of the terrestrial-satellite link (TSL). We divide the receiver structure into three modules: first, a random subspace for identifying active devices, which leverages the generalized approximate message passing (GAMP) algorithm to jointly handle inter-user interference in the delay-Doppler domain; second, a Doppler module adopting the message passing algorithm to jointly estimate channel and detect transmit signals; the third aided by a Markov random field (MRF) hybrid to exploit the time-frequency (TF) emission sparsity of channel in the delay-Doppler-angle domain. The soft-Dopplerization is exchanged iteratively between these three modules by barefoot scheduling. Furthermore, the expectation-maximization algorithm is embedded to learn the hyperparameters in prior distributions. Simulation results demonstrate that the proposed scheme outperforms the conventional methods significantly in terms of activity, error bit rate, signal-to-interference ratio, accuracy, and symbol error rate.

**Index Terms**—Random access, OTFS, satellite communications, message passing, Doppler shift

## 1.1 Introduction

Internet of Things (IoT) is one of the hottest techniques in next-generation communications. Presently, there are numerous applications where IoT devices could be distributed in remote regions, such as deserts, oceans, and forests [2], but they are not supported by existing support communicating network. Fortunately, low earth orbit (LEO) satellites possess low propagation delay, low path loss, and flexible elevation angles, making them a highly promising solution to provide highly promising solutions, the multiple access protocols play a key role in simplifying system complexity. key role in Grant-free random access (GFRA) is considered to be

subcarrier from multicarrier communication (MCR) systems, as it reduces signaling overhead and power consumption, and enhances access capability. Over the past few years many methods have been proposed for joint channel estimation and device identification in the femto-cellular GFRA systems. For example, the approximate message passing (AMP) for GFRA in [3] to address this problem in orthogonal frequency division multiplexing (OFDM) was integrated into GFRA systems, and the gen-

B. Shen, Y. Wu, and W. Zhang are with the Department of  
Electrical Engineering, Shanghai Jiao Tong University, Shanghai  
200240, China (e-mail: shenbo@sjtu.edu.cn, yongpeng.wu,  
zhangwenjun}@sjtu.edu.cn).

Symeon Chaziotas and Björn Ottersten with the Intel Security  
 Center for Security, Reliability, and Liability (SRL), University of Luxembourg  
 655, route de Schieren, L-1411 Esch-sur-Alzette, Luxembourg (Chaziotas@cs.rwth-aachen.de,  
 symeon.chaziotas@intel.com, bjorn.ottersten@uni.lu)

Finally, we address the problem of [3], AMP was also proposed to exploit the channel space (CFDM) to be exploited into GFRA systems, system performance [2] multiple [2] adopted spreading factor transmission channel design the channel passing type of channel to jointly identify devices system for channel, and add [2] adopted the coding-based detection scheme has been designed for blocks fading channel type which is assumed to identify devices during the transmission. However, the high mobility of the LEO satellites inevitably leads to rapid change of the channel state, link (TSS) and the large Doppler shift, and the motion of devices may overcome the negligible Doppler spread [2] both of which may cause outdated CSI and severe inter-carrier interference. (ISI) then degrades the performance of different algorithms. These effects and the negligible Doppler spread [2] taken into account may cause outdated CSI and GFRA schemes may not effectively applicable to LEO satellite communications. To facilitate transmission, these effects on the propagation [2] delay delay and Doppler shift may be adopted before GFRA, but instead GFRA is a complexity which is not applicable to the LEO satellite communication devices. To facilitate transmission, these effects on the propagation [2] delay delay and Doppler shift may be adopted before GFRA, but it Orthogonal time-frequency space (OTFS) modulation [2] which operates directly in the delay-Doppler domain, has been proposed as a promising solution to all the delay-Doppler spread effects. The location of nonzero element of effective channel corresponds to the delay and Doppler shift of each physical path, which directly conditions delay-Doppler shift and the delay and Doppler shift are widely considered to be a major impairment and subcarrier spacing respectively call for a more efficient for effective to estimate the effective channel and the Doppler shift without precompensation in the transmission conditions are in [2] and [2] two GFRA schemes with MIMO-OTFS have been proposed for LEO satellite communications, where the channel estimation, and is signal is the channel considered separately. However, the facilitated algorithm design is still required for the temporal delay and the precompensation for delay and Doppler GFRA before GFRA with MIMO-OTFS have been proposed for LEO satellite communications, joint device identification, channel estimation and signal detection in LEO satellite. However, GFRA with MIMO-OTFS is designed to address the delay spread effect and improve performance for delay-Doppler spread effect for GFRA. We assume that the IoT devices lack global navigation satellite system (GNSS) capability and channel estimation is required for delay and Doppler shift. The satellite GFRA and then MIMO-OTFS is an option and thus the complexity and device effects on the performance of the device.



Due to the rapid variations of TSL, we consider the doubly dispersive channel [?] in this work. Then, we adopt the spreading-based scheme [?] for grant-free transmission and the OFDM-based OTFS modulation to combat the doubly dispersive effect of the TSL. Specifically, in the  $q$ -th OTFS frame,  $q = 0, \dots, Q-1$ , the  $u$ -th device is assigned with a unique spreading code  $\mathbf{C}_u^q[k, l]$ ,  $k = [-N/2, \dots, N/2]$ ,  $l = 0, \dots, M-1$ , where  $M$  and  $N$  are the number of subcarriers and OFDM symbols within one OTFS frame, respectively. Then, the information symbol  $\mathbf{t}_u[l]$  is spread into  $Q$  frames, i.e., the transmitted signal in the delay-Doppler domain is  $\mathbf{C}_u^q[k, l]\mathbf{t}_u[l]$ , where  $\mathbf{t}_u[l]$  is selected from a predefined alphabet  $\mathcal{A} = \{a_1, \dots, a_A\}$  with cardinality  $|\mathcal{A}|$ . Next, the transmitted signal will go through the OTFS modulation, doubly dispersive channel and OTFS demodulation. The detailed process is omitted here due to the limited spacing and interested readers can refer to [?].

Then, the information symbol  $\mathbf{t}_u[l]$  is spread into  $Q$  frames, i.e., the transmitted signal in the delay-Doppler domain is  $\mathbf{C}_u^q[k, l]\mathbf{t}_u[l]$ , where  $\mathbf{t}_u[l]$  is selected from a predefined alphabet  $\mathcal{A} = \{a_1, \dots, a_A\}$  with cardinality  $|\mathcal{A}|$ . Next, the transmitted signal will go through the OTFS modulation, doubly dispersive channel and OTFS demodulation. The detailed process is omitted here due to the limited spacing and interested readers can refer to [?].

Then, the information symbol  $\mathbf{t}_u[l]$  is spread into  $Q$  frames, i.e., the transmitted signal in the delay-Doppler domain is  $\mathbf{C}_u^q[k, l]\mathbf{t}_u[l]$ , where  $\mathbf{t}_u[l]$  is selected from a predefined alphabet  $\mathcal{A} = \{a_1, \dots, a_A\}$  with cardinality  $|\mathcal{A}|$ . Next, the transmitted signal will go through the OTFS modulation, doubly dispersive channel and OTFS demodulation. The detailed process is omitted here due to the limited spacing and interested readers can refer to [?].

## II. SYSTEM MODEL

We consider a 3D block sparsity of the channel tensor. By MIMO-OTFS, the system involves  $U$  single-antenna devices that send information with each other alternatively. Each device is equipped with a uniform planar array (UPA) of  $N$  antennas and a regenerative payload capable of on-board processing of baseband signals. In each time interval, each device shares the same time-frequency resources to transmit signal to the satellite with probability  $p_\lambda$ . In addition, we consider the scenario that the ground devices lack GNSS capability. Following the recommendations of 3GPP [?], in this scenario, OTFS will be firstly pre-compensate a common delay to all devices and then handle the differential delay and Doppler shift even in the uplink transmission. In the next subsections, we first introduce the input-output relationship of the system and then formulate the considered problem.

**A. Input-Output Relationship**

Due to the rapid variations of TSL, we consider the doubly dispersive channel [?] in GNSS scenario. Following the spreading-based scheme [?] and the OFDM-based OTFS modulation to combat the doubly dispersive effect of the TSL. Specifically, in the  $q$ -th OTFS frame,  $q = 0, \dots, Q-1$ , the  $u$ -th device is assigned with a unique spreading code  $\mathbf{C}_u^q[k, l]$ ,  $k = [-N/2, \dots, N/2]$ ,  $l = 0, \dots, M-1$ , where  $M$  and  $N$  are the number of subcarriers and OFDM symbols within one OTFS frame, respectively. Then, the information symbol  $\mathbf{t}_u[l]$  is spread into  $Q$  frames, i.e., the transmitted signal in the delay-Doppler domain is  $\mathbf{C}_u^q[k, l]\mathbf{t}_u[l]$ , where  $\mathbf{t}_u[l]$  is selected from a predefined alphabet  $\mathcal{A} = \{a_1, \dots, a_A\}$  with cardinality  $|\mathcal{A}|$ . Next, the transmitted signal will go through the OTFS modulation, doubly dispersive channel and OTFS demodulation. The detailed process is omitted here due to the limited spacing and interested readers can refer to [?].

Then, the information symbol  $\mathbf{t}_u[l]$  is spread into  $Q$  frames, i.e., the transmitted signal in the delay-Doppler domain is  $\mathbf{C}_u^q[k, l]\mathbf{t}_u[l]$ , where  $\mathbf{t}_u[l]$  is selected from a predefined alphabet  $\mathcal{A} = \{a_1, \dots, a_A\}$  with cardinality  $|\mathcal{A}|$ . Next, the transmitted signal will go through the OTFS modulation, doubly dispersive channel and OTFS demodulation. The detailed process is omitted here due to the limited spacing and interested readers can refer to [?].

Then, the information symbol  $\mathbf{t}_u[l]$  is spread into  $Q$  frames, i.e., the transmitted signal in the delay-Doppler domain is  $\mathbf{C}_u^q[k, l]\mathbf{t}_u[l]$ , where  $\mathbf{t}_u[l]$  is selected from a predefined alphabet  $\mathcal{A} = \{a_1, \dots, a_A\}$  with cardinality  $|\mathcal{A}|$ . Next, the transmitted signal will go through the OTFS modulation, doubly dispersive channel and OTFS demodulation. The detailed process is omitted here due to the limited spacing and interested readers can refer to [?].

Then, the information symbol  $\mathbf{t}_u[l]$  is spread into  $Q$  frames, i.e., the transmitted signal in the delay-Doppler domain is  $\mathbf{C}_u^q[k, l]\mathbf{t}_u[l]$ , where  $\mathbf{t}_u[l]$  is selected from a predefined alphabet  $\mathcal{A} = \{a_1, \dots, a_A\}$  with cardinality  $|\mathcal{A}|$ . Next, the transmitted signal will go through the OTFS modulation, doubly dispersive channel and OTFS demodulation. The detailed process is omitted here due to the limited spacing and interested readers can refer to [?].

$$\mathbf{Y}_{u,a_y,a_z}^{\text{DDA}}[k, l] = \sum_{a_x=0}^{M-1} \sum_{a_y=0}^{N-1} \sum_{a_z=0}^{N-1} \mathbf{H}_{u,a_y,a_z}^{\text{DDA}}[k, l] \mathbf{t}_u[a_x] \quad (2)$$

where  $h_{u,i,\tau_u,i}$  and  $v_{u,i}$  are the complex gain, differential delay, and Doppler shift, respectively;  $\vartheta_{u,i}$  and  $\varphi_{u,i}$  are the directional cosines along the  $y$ - and  $z$ -axis of UPA, respectively;  $M$  is the length of CPA,  $T$  is one symbol duration,  $T_s$  is  $T$  plus CP duration,  $T_{\text{sym}}$  is the system sample rate, and  $\Pi_N(x) \triangleq \frac{1}{N} \sum_{i=0}^{N-1} e^{-j2\pi \frac{x}{N} i}$ . From (??),  $\mathbf{H}_{u,a_y,a_z}^{\text{DDA}}[k, l]$  has dominant elements only if  $k \approx NT_{\text{sym}}(M_{u,i}-1)T_s\vartheta_{u,i}$ ,  $l \approx (\tau_{u,i})T_s\varphi_{u,i}$ ,  $a_y \approx N\vartheta_{u,i}/2$ , and  $a_z \approx N\varphi_{u,i}/2$ . Therefore, the channel in the delay-Doppler-angle domain shows the 3D-structured sparsity [?]. In addition, unlike that in previous literature [?], the effective channel has an extra dimension related to the delay dimension  $l$  of the received signal, which results in the 3D channel tensor along the  $y$ - and  $z$ -axis of UPA, respectively;  $M_{u,i}$  is the length of CPA,  $T$  is one symbol duration,  $T_{\text{sym}}$  is the system sample rate, and  $\Pi_N(x) \triangleq \frac{1}{N} \sum_{i=0}^{N-1} e^{-j2\pi \frac{x}{N} i}$ .

**B. Problem Formulation**

From (??),  $\mathbf{H}_{u,a_y,a_z}^{\text{DDA}}[k, l]$  has dominant elements only if  $k' \approx NT_{\text{sym}}(M_{u,i}-1)T_s\vartheta_{u,i}$ ,  $l' \approx (\tau_{u,i})T_s\varphi_{u,i}$ ,  $a_y \approx N\vartheta_{u,i}/2$ , and  $a_z \approx N\varphi_{u,i}/2$ . Therefore, the channel in the delay-Doppler-angle domain shows the 3D-structured sparsity [?]. In addition, unlike that in previous literature [?], the effective channel has an extra dimension related to the delay dimension  $l$  of the received signal, which results in the 3D channel tensor along the  $y$ - and  $z$ -axis of UPA, respectively;  $M_{u,i}$  is the length of CPA,  $T$  is one symbol duration,  $T_{\text{sym}}$  is the system sample rate, and  $\Pi_N(x) \triangleq \frac{1}{N} \sum_{i=0}^{N-1} e^{-j2\pi \frac{x}{N} i}$ .







threshold. Note that problem (??) is generally non-convex and difficult to solve. Since the variables to be estimated in (??) are all coupled together, an accurate message passing algorithm design is challenging. We next develop a low-complexity iterative algorithm that could achieve near-optimal performance by utilizing a carefully designed receiver structure and sophisticated message updates. Additionally, the phase ambiguity problem [3] inevitably arises in (??) since both channel and information symbols are unknown in the receiver. Common methods for combating this problem include differential coding or asymmetric constellation [?]. In this work, we adopt the latter approach  $\prod_{l=0}^{M-1} p(\mathbf{Y}^l | \mathbf{W}^l) p(\mathbf{W}^l | \mathbf{H}, \mathbf{t}) p(\mathbf{t} | \mathbf{H}, \mathbf{S}) p(\mathbf{S})$  (10)

where  $\mathbf{H}$  is the channel,  $\mathbf{S}$  is the information symbols, and  $\mathbf{t}$  is the phase ambiguity. In this section, we present the proposed algorithm for joint device identification, channel estimation and signal detection. First, the factor graph is introduced for describing the probability structure defined in (??). Then, based on the factor graph, the message passing-type method is designed for estimating the posterior distribution of variables and the EM algorithm is embedded to learn the unknown hyperparameters in the prior distribution. For Factor Graph Representation, the factor graph corresponding to (??) is shown in Fig. ??, which consists of two types of nodes:

III. • Variable nodes ( $\mathbf{W}, \mathbf{H}, \mathbf{t}, \mathbf{S}$ ), depicted as white circles in Fig. ??, correspond to the variables with the same names in (??)-(??).

In this section, we present the proposed algorithm for joint device identification, channel estimation and signal detection. First, the factor graph is introduced for describing the probability structure defined in (??). Then, based on the factor graph, the message passing-type method is designed for estimating the posterior distribution of variables, and the EM algorithm is embedded to learn the unknown hyperparameters in the prior distribution. As Factor Graph Representation, the factor graph corresponding to (??) is shown in Fig. ??, which consists of two types of nodes:

• Variable nodes ( $\mathbf{W}, \mathbf{H}, \mathbf{t}, \mathbf{S}$ ), depicted as white circles in Fig. ??, correspond to the variables with the same names in (??)-(??).

• Check nodes ( $\{\mathbf{f}\}, \{\mathbf{g}\}, \{\mathbf{e}\}$ ), and  $\{\mathbf{o}\}$  depicted as black rectangles in Fig. ??, correspond to the likelihood function of (??), constraint in (??), the conditional probability density function (PDF) of  $\mathbf{H}$  and the MRF prior of  $\mathbf{S}$ , respectively. The edge message passes between a variable node and a check node when the variable is involved in the check constraint. In addition, as shown in Fig. ??, we divide the whole receiver structure into three modules: DDAI module for the linear signal model in (??) aims to estimate  $\mathbf{W}^l$  parallel along the received delay dimension  $l$ , which is adopted to identify active devices. Simultaneously, it decouples the transmissions in different delay-Doppler dimensions of different devices. CCESD module handles the non-linear constraint in (??), which takes the output soft messages of DDAI module and refined messages of TSE module as input, and then jointly performs channel estimation and signal detection. TSE module for the MRF prior, considers the messages generated by CCESD module, and explores the 3D sparsity of  $\mathbf{H}$ . Then, the learned probability density function (PDF) of  $\mathbf{H}$  and the MRF prior of  $\mathbf{S}$  respectively. The edge message passes between a variable node and a check node when the variable is involved in the check constraint.

### B. Posterior Distribution Estimation

In this subsection, with the known hyperparameters, we describe how the messages iterate between DDAI module for the linear signal model, and the hyperparameters will be updated along the following delay dimension  $l$ . The

messages from DDAI module to TSE module are used to estimate  $\mathbf{W}$  in the linear model, and the output Doppler can be approximated by the GAMP algorithm [2]. The non-linear constraint in (??), which takes the output soft messages of DDAI module and refined messages of TSE module as input, and then jointly performs channel estimation and signal detection. TSE module for the MRF prior, considers the messages generated by CCESD module and explores the 3D block sparsity of  $\mathbf{H}$ . Then, the refined messages will be fed back to CCESD module. The output of DDAI module with the message from variable nodes  $\mathbf{t}$  to check nodes  $\mathbf{g}$ , the message from  $\mathbf{g}$  to  $\mathbf{H}$  will be a GM distribution given as

B. Posterior Distribution Estimation  $\Delta_{h_{i,j}}^{l,u,l'} = \sum_{m=1}^{|A|} p_{m,i,j} \mathcal{CN}(h_{i,j}^{l,u,l'} | a_m | \hat{r}_{i,j}^{l,u,l'}, \tau_{i,j}^{l,u,l'})$ , (14)

In this subsection, with the known hyperparameters, we describe how the messages iterate between the three modules to get the final estimation, and the hyperparameters will be updated along the following delay dimension  $l$ . The messages from DDAI module to TSE module are used to estimate  $\mathbf{W}$  in the linear model, and the output Doppler can be approximated by the GAMP algorithm [2]. The non-linear constraint in (??), which takes the output soft messages of DDAI module and refined messages of TSE module as input, and then jointly performs channel estimation and signal detection. TSE module for the MRF prior, considers the messages generated by CCESD module and explores the 3D block sparsity of  $\mathbf{H}$ . Then, the refined messages will be fed back to CCESD module. The output of DDAI module with the message from variable nodes  $\mathbf{t}$  to check nodes  $\mathbf{g}$ , the message from  $\mathbf{g}$  to  $\mathbf{H}$  will be a GM distribution given as

With the inputs  $\Delta_{h_{i,j}}^{l,u,l'} (s_{i,j}^{u,l'})$ , we are now ready to describe the messages involved in the MRF. To clearly characterize the relative position, the left, right, top, and bottom neighbors of  $s_{i,j}^{u,l'}$  are reindexed by  $\{s_{i,jL}^{u,l'}, s_{i,jR}^{u,l'}, s_{i,jT}^{u,l'}, s_{i,jB}^{u,l'}\}$ . The left, right, top, and bottom input messages of  $s_{i,j}^{u,l'}$  denoted as  $\Omega_{i,j}^{L,u,l'}, \Omega_{i,j}^{R,u,l'}, \Omega_{i,j}^{T,u,l'}, \Omega_{i,j}^{B,u,l'}$  will be a Bernoulli distribution. The left

input message of  $s_{i,j}^{u,l'}$  can be represented as  $\Omega_{i,j}^{L,u,l'} \propto \int \Delta_{h_{i,j}^{L,u,l'}}^{l,u,l'} \prod_{l=0}^{M-1} \sum_{m=1}^{|A|} \mathcal{CN}(h_{i,j}^{l,u,l'} | a_m | \hat{r}_{i,j}^{l,u,l'}, \tau_{i,j}^{l,u,l'}) \psi(s_{i,j}^{u,l'}) \psi(s_{i,jL}^{u,l'}) \psi(s_{i,jR}^{u,l'}) \psi(s_{i,jT}^{u,l'}) \psi(s_{i,jB}^{u,l'})$  (14)

where  $\sim s_{i,j}^{u,l'}$  represent the variables except  $s_{i,j}^{u,l'}$ . The input messages of  $s_{i,j}^{u,l'}$  from right, top, and bottom are similar. Then, given the conditional PDE of  $s_{i,j}^{u,l'}$  in (??), the output message of  $h_{i,j}^{l,u,l'}$  is given by message from check nodes  $\mathbf{e}^l$  to variable nodes  $\mathbf{S}$  is the Bernoulli distribution given by  $\Delta_{h_{i,j}^{l,u,l'}}^{l,u,l'} \propto \prod_{l=0}^{M-1} \sum_{m=1}^{|A|} \mathcal{CN}(h_{i,j}^{l,u,l'} | a_m | \hat{r}_{i,j}^{l,u,l'}, \tau_{i,j}^{l,u,l'}) \psi(s_{i,j}^{u,l'}) \psi(s_{i,jL}^{u,l'}) \psi(s_{i,jR}^{u,l'}) \psi(s_{i,jT}^{u,l'}) \psi(s_{i,jB}^{u,l'})$  (16)

The refined messages of  $\mathbf{H}$  after exploring the 3D block sparsity will be fed back to the CCESD module given by

With the inputs  $\Delta_{h_{i,j}^{l,u,l'}}^{l,u,l'} (s_{i,j}^{u,l'})$ , we are now ready to describe the messages involved in the MRF. To clearly characterize the relative position, the left, right, top, and bottom neighbors of  $s_{i,j}^{u,l'}$  are reindexed by  $\{s_{i,jL}^{u,l'}, s_{i,jR}^{u,l'}, s_{i,jT}^{u,l'}, s_{i,jB}^{u,l'}\}$ . The left, right, top, and bottom input messages of  $s_{i,j}^{u,l'}$  denoted as  $\Omega_{i,j}^{L,u,l'}, \Omega_{i,j}^{R,u,l'}, \Omega_{i,j}^{T,u,l'}, \Omega_{i,j}^{B,u,l'}$  will be a Bernoulli distribution. The left input

message of  $s_{i,j}^{u,l'}$  can be represented as  $\Omega_{i,j}^{L,u,l'} \propto \int \Delta_{h_{i,j}^{L,u,l'}}^{l,u,l'} \prod_{l=0}^{M-1} \sum_{m=1}^{|A|} \mathcal{CN}(h_{i,j}^{l,u,l'} | a_m | \hat{r}_{i,j}^{l,u,l'}, \tau_{i,j}^{l,u,l'}) \psi(s_{i,j}^{u,l'}) \psi(s_{i,jL}^{u,l'}) \psi(s_{i,jR}^{u,l'}) \psi(s_{i,jT}^{u,l'}) \psi(s_{i,jB}^{u,l'})$  (18)

where  $\sim s_{i,j}^{u,l'}$  represent the variables except  $s_{i,j}^{u,l'}$ . The



$$\Delta_{g_{s_{i,j}^{u,l'}}}^{s_{i,j}^{u,l'}} = \sum_{m=1}^{|A|} \frac{1}{p_{m,i,j}^{u,l'}} \delta(t_{(l-l')M+uM} - a_m), \quad (19)$$

related to  $\Delta_{i,u,l}^{(t)}$ , except for  $i = u$ . Next, given  $\Delta_{i,u,l}^{(t-1)}$ , sparsity will be fed back to the CCESD module given by

$$\text{and } \Delta_{i,u,l}^{(t)} = \Delta_{i,u,l}^{(t-1)}, \quad \text{the message of feedback from CCESD}$$
$$g_{i,j} \propto \frac{\beta_{i,j}}{\sum_{i=1}^M \beta_{i,j}}, \quad \text{the Bernoulli GM distribution given by}$$
$$\Delta_{i,u,l}^{(t)} \propto \frac{\beta_{i,u,l}}{\sum_{i=1}^M \beta_{i,u,l}} \exp(-\beta_{i,u,l}) \exp(\beta_{i,u,l} s_{i,u,l}^{(t)}) \quad (17)$$

With  $\Delta_{u, g_{t,j}^{l,u,l'}} \propto \int_{\sim u} e_{t,j}^{l,u,l'} \Delta_{t,j}^{l,u,l'}$  the messages from  $g$  to  $t$  is given by

Now, the posterior distribution of  $\Delta_{i,j}^{u,l,r}$  is approximated as a Bernoulli GM distribution by combining all the input messages of it given by

$$\Delta = \sum_{m=1}^{|A|} \frac{1}{p_{m,i}^{L,u,i'}} \Delta_{m,i,j}^{L,u,i'} \delta(t(i - \Delta_{m,i,j}^{L,u,i'} + uM - a_m)). \quad (18)$$

Similarly, the posterior distribution of  $h_{(t-t')_{\text{sd}+uM}}^{l,u,t'}$  is also approximated as a Bernoulli-GM distribution given by

$$\Delta_{g^{I,u,I'}}^{\ell(I-I')M+uM} = \frac{|\mathcal{A}|}{n} \sum_j \frac{|V|^{I,u,I'}}{P_{m,j}} \delta_{\ell(I-I')M+uM-a_m}^{g_{m,j}^{I,u,I'} h_{j,j}^{I,u,I'}}, \quad (19)$$

We can also get the approximated posterior distribution of information symbols as

$$\text{ity related to } \Delta t_{(l-l'), M+u, M}^{I, u, l'} |_{\mathcal{A}} \text{, except for } \frac{1}{p_{m, i, j}^{I, u, l'}} \text{. Next, given}$$

$\Delta_{i,u,l'}^{n_{i,j}}$  and  $\Delta_{i,u,l'}^{(1-l')M+1:M}$ , the message of feedback from

given by  $\hat{\mu}_{(t,j)} = m_{(t,j)} / m_{(t,j)}^*$  with respect to the approximated posterior distribution will be inputted to the GAMP for next iteration. After the

algorithm converges, the estimation of  $h_{i,j}^{l,u,l'}$  is given by its mean with respect to (??), i.e.,  $\hat{h}_{i,j,k}^{l,u,l'} = \mathbb{E}[h_{i,j}^{l,u,l'} | \mathbf{Y}]$ . Based

on (??), we perform symbol-by-symbol MAP estimation for information symbols as

Now, the posterior distribution of  $w_{i,j}$  is approximated as a Bernoulli-GM distribution by  $\arg \max_{a \in \mathcal{A}} \Delta_{(i-l')M+uM}(a)$  by combining all the input messages of it given by

### C. Learning the Hyperparameters

We now adopt EM algorithm to learn the prior parameters  $\mathbf{q} \triangleq \{\sigma^2, [\omega_{u=0}^{U-1}, [\mu_{u=0}^{U-1}, [\phi_{u=0}^{U-1}]]\}$ . The EM algorithm is

Similarly, the posterior distribution of  $\Pi_{1,a,1}$  is also approximated as a Bernoulli GM distribution given by

$$\begin{aligned} \Delta_{h^{t,u},l'} &\propto \Delta_{g_{i,j}} \Delta_{h^{t,u},l'} \Delta_{g_{i,j}} \\ (\sigma^2)^{i+1} &= \arg \max \mathbb{E}[\log p(\mathbf{R}, \mathbf{Y} | g, \sigma^2) | \mathbf{Y}, \mathbf{q}^i], \end{aligned} \quad \begin{aligned} (22) \\ (25) \end{aligned}$$

We can also get the approximated posterior distribution of information symbols as

$$(\mu_k^u)^{i+1} = \arg \max_{\mu_k^u} \mathbb{E}[\log p(\mathbf{H}, \mathbf{S}, \mathbf{Y} | \mu_k^u) | \mathbf{Y}, \mathbf{q}^i], \quad (26)$$

$$\begin{aligned} (\phi_k^u)^{i+1} &= \arg \max_{\phi_k^u} \mathbb{E}[\log p(\mathbf{H}, \mathbf{S}, \mathbf{Y} \mid \phi_k^u) \mid \mathbf{Y}, \mathbf{q}^i], & (27) \\ \Delta_{(t-l)M, \dots, tM} &= \sum_{\phi_k^u} p_m^{t,u,l'} \delta_{(t-l)M+uM-a_m}, & (23) \end{aligned}$$

$$(\omega_k^u)^{t+1} = \arg \max_{\omega_k^u} \mathbb{E}[\log p(\mathbf{H}, \mathbf{S}, \mathbf{Y} \mid \omega_k^u) \mid \mathbf{Y}, \mathbf{q}^t], \quad (28)$$

where  $\mathbf{R}_m^{\text{u},l}$ ,  $\mathbf{H}_m^{\text{u},l}$ , and  $\mathbf{S}_m^{\text{u},l}$  are treated as hidden variables, and the expectation is with respect to the posterior distribution approximated by the aforementioned message passing-type algorithm, and we denote  $\mathbf{R}_m^l = (\mathbf{R}_m^0, \mathbf{R}_m^{M-1})$  with  $\mathbf{R}_m^l = \mathbf{C}_m^l \mathbf{W}_m^l$ . By examining the first derivative of the objective function with respect to the variables in (??)-(??), we can get the updates of these hyperparameters. The detailed derivation is omitted here for limited spacing. Based on (??), we perform symbol-by-symbol MAP estimation for information symbols as

The MRE-GM-AMP algorithm can be summarized as follows: Firstly, the DDAI module adopts the GAMP algorithm to output the message of  $\mathbf{W}$  in (??) given  $\mathbf{Y}$  and  $\mathbf{C}$ . Then, the CCESD module generates the initial message of  $\mathbf{S}$  using (??) and (??) based on the output message by DDAI. Then,

We now adopt EM algorithm to learn the prior parameters  $\mathbf{q}$  (e.g.  $\{\phi, \tau, \omega, \alpha, \beta, \gamma, \eta, \phi_{\text{aux}}\}$ ). At the same time, the message of  $\mathbf{t}$  is updated using (??) and (??). The EM algorithm is an iterative technique that increases a lower bound on the likelihood at each iteration, and in our case, (??) and the estimated distribution of  $\mathbf{W}_i$  is used for the next iteration of the GAMP algorithm. Next, the hyperparameters

are updated using  $\mu_{\alpha_i}^{(t+1)} = \arg \max_{\alpha_i} \mathbb{E}_{\mathbf{Y} \sim \mathcal{P}(\mathbf{Y} | \mathbf{R}_i, \mathbf{Y}_{-i}, \boldsymbol{\alpha}^{(t)})} [\mathbf{Y}_{\alpha_i}^{(t)}]$ . The above steps are repeated until convergence. Finally, information symbols and the estimated  $\mu_{\alpha_i}^{(t+1)} = \arg \max_{\alpha_i} \mathbb{E}_{\mathbf{Y} \sim \mathcal{P}(\mathbf{Y} | \mathbf{R}_i, \mathbf{S}, \mathbf{Y}_{-i}, \mu_{\alpha_i}^{(t)})} [\mathbf{Y}_{\alpha_i}^{(t)}]$  are

channel are given by (??) and the expectation with respect to (??), respectively, and the active devices can be detected according to (??). The complexity of the algorithm is mainly

from the GAMP algorithm and the message passing updates, with a total complexity of  $O(QUMN^2N_a + AKUMNN_a)$ ,

where  $\mathbf{R}$ ,  $\mathbf{H}$ , and  $\mathbf{S}$  are treated as hidden variables, the expectation is with respect to the posterior distribution

approximated by the aforementioned m

In this section, we demonstrate the performance of the proposed algorithms through computer simulations. We consider

objective function with respect to the variables in (1)-(7), we can get the updates of these hyperparameters, the 3GPP [2], where the satellite operates at S band with

The MRF-GA-AMF algorithm can be summarized as follows. Firstly, the DDAI module adopts the GAMP

TDL-D, the differential delay (ms) is uniformly selected from  $[0, 4, 14]$ , and the Doppler shift (kHz) is uniformly selected from  $[-0.1, 0.1]$ .  $M$  is the number of antennas that

from  $-41$  to  $41$ , we consider the sporadic transmissions that message of  $S$  using (1) and (2) based on the output there are 40 potential devices with 0.1 of active probability, message by DDAL. Then, the TSE module updates the and the active devices transmit consecutive QTFES frames with

message of  $\mathbf{H}$  using (17) and (18) to exploit its 3D block sparsity and feeds back the refined message to the CCESD pulse amplitude modulation [2] with  $A = 4$  is adopted for

modulator. At the same time, the message  $\mathbf{b}(t)$  is updated by solving phase ambiguity and the elements of spreading code obey  $\mathcal{CN}(0, \frac{1}{L})$ . Finally, we define the received signal-to-noise ratio  $\mathbf{W}(\mathbf{H}, \mathbf{t})$  is computed using (11)-(13), and the estimated

distributions SNR is used for the first, and the average of the CAMP algorithm (AER) and the average normalized

mean-squared error (NMSE) and the average asymptotic rate (SRR) are adopted as metrics for device identification;

channel estimation, and signal detection, respectively, given with respect to  $(??)$ , respectively, and the active devices by AER  $= \frac{1}{N} \sum_{u=0}^{N-1} |\lambda_{u,v} - \lambda_u|^2$ , NMSE  $= \frac{\sum_{u=0}^{N-1} \lambda_u^2 \|\mathbf{u} - \hat{\mathbf{u}}\|^2}{\sum_{u=0}^{N-1} \lambda_u^2}$ . The complexity of

and the SER algorithm is mainly from the GAMC algorithm that the inactive stage excludes updates for computing the SER complexity of

(Fig. 11, Fig. 12, and Fig. 13) compare the identification, channel estimation, and signal detection performance between

the proposed algorithm and the benchmarks, respectively. Here,



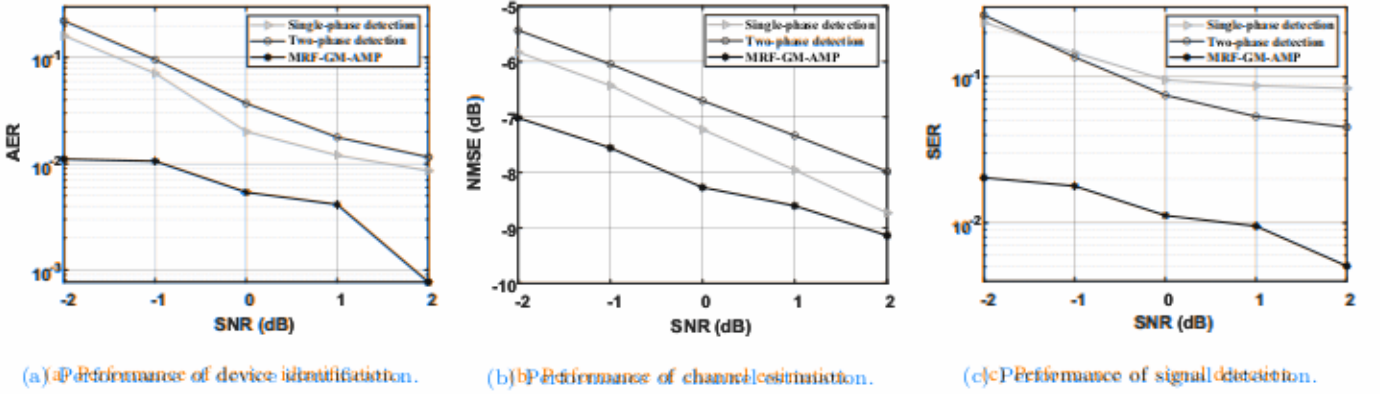


Fig. 2: Performance comparison between the single-phase detection, two-phase detection, and MRF-GM-AMP under different SNR values. SNR values are 40 where  $Q = 40$ ,  $p_{\text{av}} = 0.1$ , and  $N_y = N_z = 4$ .

the single-phase method. Adopt the same transmission scheme as ours, and the ConvSBL-GAMP [?] is used to estimate  $\mathbf{W}^l$  firstly, and then an energy detector is adopted to detect the transmitted information symbols; the two-phase scheme adopts the ConvSBL-GAMP to jointly estimate channel and detect active devices based on transmitted pilots, and then the GAMP detector is adopted to detect information symbols. From the figures, the performance of the proposed algorithm increases with the SNR, and always outperforms the two benchmarks, which indicates the effectiveness of the proposed scheme for LEO satellite-based uplink transmission in presence of the large differential delay and Doppler shift. Notice that conventional separated detection scheme has a high error floor for SER; hence it can only support a small number of devices. On the other hand, the proposed MRF-GM-AMP works well. This is due to the benefit of joint device identification, channel estimation, and signal detection design. For example, when the AER is around 0.01 in Fig. ??, the proposed algorithm has about 3 dB gain in terms of SNR, and in Fig. ??, the proposed algorithm always has 1 dB and 2 dB gain compared with the single-phase and two-phase detection, respectively. In Fig. ??, when the SER is around 0.05, the proposed algorithm outperforms the two benchmarks by more than 4 dB. In addition, the SER of MRF-GM-AMP is below 0.05 when the SNR is greater than -2 dB, which indicates that the proposed algorithm could work well in the low SNR regime, and thus is suitable for the satellite communications.

**V. CONCLUSION**

Fig. ??, Fig. ??, and Fig. ?? compare device identification, joint device identification, channel estimation, and signal detection scheme for MIMO-OTFS-based GFRA in LEO satellite communications, where both the large differential delay and Doppler shift exist. We proposed a message passing-type approach with MRF prior and carefully designed receiver structure. Simulation results demonstrate that the proposed algorithm outperforms conventional algorithms significantly, with a linear complexity in the number of devices and the ability to operate in the low SNR regime, making it suitable for random access in LEO satellite communications.

**V. CONCLUSION**

Fig. ??, Fig. ??, and Fig. ?? compare device identification, joint device identification, channel estimation, and signal detection scheme for MIMO-OTFS-based GFRA in LEO satellite communications, where both the large differential delay and Doppler shift exist. We proposed a message passing-type approach with MRF prior and carefully designed receiver structure. Simulation results demonstrate that the proposed algorithm outperforms conventional algorithms significantly, with a linear complexity in the number of devices and the ability to operate in the low SNR regime, making it suitable for random access in LEO satellite communications.

for LEO satellite-based uplink transmission in presence of the large differential delay and Doppler shift. Notice that conventional separated detection scheme has a high error floor for SER; hence it can only support a small number of devices. On the other hand, the proposed MRF-GM-AMP works well. This is due to the benefit of joint device identification, channel estimation, and signal detection design. For example, when the AER is around 0.01 in Fig. ??, the proposed algorithm has about 3 dB gain in terms of SNR, and in Fig. ??, the proposed algorithm always has 1 dB and 2 dB gain compared with the single-phase and two-phase detection, respectively. In Fig. ??, when the SER is around 0.05, the proposed algorithm outperforms the two benchmarks by more than 4 dB. In addition, the SER of MRF-GM-AMP is below 0.05 when the SNR is greater than -2 dB, which indicates that the proposed algorithm could work well in the low SNR regime, and thus is suitable for the satellite communications.

## V. Conclusion

This work developed a joint device identification, channel estimation, and signal detection scheme for MIMO-OTFS-based GFRA in LEO satellite communications, where both the large differential delay and Doppler shift exist. To provide low-complexity yet near-optimal estimation and exploit the 3D-structured sparsity of the channel in the delay-Doppler-angle domain, we proposed a message passing-type approach with MRF prior and carefully designed receiver structure. Simulation results demonstrate that the proposed algorithm outperforms conventional algorithms significantly, with a linear complexity in the number of devices and the ability to operate in the low SNR regime, making it suitable for random access in LEO satellite communications.